REMARKS

Claims 39-53 and 67-74 are currently pending in the application. The Board Decision Appeal 2008-1316 ("the Board Decision") affirmed the Examiner's rejection of claims 39-53 and 67-74 under 35 U.S.C. § 102(e) as anticipated by Whitcher. The Board Decision was mail dated June 17, 2009 and the Applicant submits herewith a Request for Continued Examination within the two month time period for reply. Applicant submits a submission subsequently recited herein, and respectfully request reconsideration and further examination of the present application under 37 C.F.R. §1.112.

ARGUMENTS

A. 35 U.S.C. § 102(e) rejection of pending claims 39-53 and 67-74 as being anticipated by Whitcher et al. (U.S. Pub. No. US 2003/0018381).

The pending application is directed towards a method of manufacturing an endoluminal stent. More specifically, the claimed method (as recited in independent claims 39, 47, and 67 of the Application) requires, *inter alia*, the step of vacuum depositing a stent-forming metal onto a substrate under process conditions selected to minimize (or substantially eliminate) formation of chemical and intra- and inter-granular precipitates in the bulk material of the as deposited crystalline film.

The Board Decision stated that Whitcher explicitly describes deposition of monocrystalline and nanocrystalline metallic films (Board Decision, FF 15). The term nanocrystalline is undefined in *Whitcher*; however, it is generally understood to simply be nano-scale polycrystalline structures. (*See, e.g.*, Hollister, P., et al., Nanocrystalline Materials, Technology White Papers nr. 4, Cientifica, Oct. 2003, nanotechweb.org/dl/wp/nanocrystalline_materials_WP.pdf, a copy of which is attached as Exhibit A). The term "monocrystalline" is also undefined in *Whitcher*. However, that term is generally understood to mean "formed of a single crystal-unit, and so all elements have identical crystallographic orientation of c- and a-axes and overgrow as one unit." (*See*, <www.nhm.ac.uk/hosted_sites/ina/terminology/7crystallography.htm>.) Monocrystalline (a/k/a single crystal) materials as taught by *Whitcher* as drawn filaments and are not, therefore, vacuum deposited onto a cylindrical substrate to form a tubular film structure. And nano-scale crystal structures are desirable to enhance mechanical properties of the medical device, and have

nothing to do with precipitates. As such, *Whitcher* does not disclose, expressly or implicitly, that vacuum deposition may be controlled to minimize formation of precipitates in the as-deposited crystalline film.

The Board Decision stated that Whitcher describes a vacuum deposition process for controlling the composition, thickness, surface roughness, and microstructure" of the medical devices" and impart "desired compositions, mechanical properties, and geometries" (Board Decision, FF 11, 12). Applicant submits that the concept of controlling aspects of the microstructure of a deposited metal is different from the concept of minimizing precipitates in a deposited metal film. As widely known to those skilled in the metallurgical arts, the term "precipitate[1]" is different from the term "microstructure[2]" and different from the term "impurity[3]." In the metallurgical arts as they pertain to fabrication of biomaterials, and with particular reference to nickel-titanium shape memory alloys, precipitates are reaction products formed from a solid solution under increased thermal conditions which drive the precipitate from solution, resulting in formation of the reaction products outside the solid solution, *i.e.*, the metal crystalline structure. An excellent monograph on precipitation reactions in nickel-titanium binary shape memory alloy systems is found at Pelton, A.R., et al., Optimisation of processing and properties of medical grade Nitinol Wire, *Min Invas Ther & Allied Techno.*, 2000: 9(1) 107–118, a copy of which is attached as Exhibit B.

Thus, a "precipitate" is not an "impurity." Rather, it is a reaction product from the solid metal solution. Conversely, an "impurity" is not a "precipitate". Indeed, on paragraph 37, *Whitcher* clearly notes that "other impurities, such as oxygen, that may be contained in the elemental ingot may be filtered away from the substrate with this method" [Emphasis added]. Based on Applicant's meticulous reading, there is no description whatsoever in *Whitcher* indicating that the "impurities" described in *Whitcher* and referenced by the Examiner, actually refer to precipitates.

Additionally, the Board Decision stated that no working examples or specific vacuum

---

[1] Online website <www.dictionary.com> defines the term precipitate as "a substance precipitated from a solution" and "to separate (a substance) in solid form from a solution, as by means of a reagent."

[2] Online website <www.dictionary.com> defines the term microstructure as "the structure of a metal or alloy as observed, after etching and polishing, under a high degree of magnification."

[3] Online website <www.dictionary.com> defines the term impurity as "the quality or state of being impure."

deposition conditions are described in the Specification (FF8). However, the present application states "[a]s is described in co-pending, commonly assigned, U.S. Patent Application Serial No. 09/443,929, filed November 19, 1999, which is hereby incorporated by reference, heterogeneities are controlled by fabricating the bulk material of the stent to have defined grain sizes, chemical and intra and intergranular precipitates and where the bulk and surface morphology differ, yielding areas or sites along the surface of the stent while maintaining acceptable or optimal protein binding capability. Present Application, page 10, lines 24-30. The U.S. Patent Application Serial No. 09/443,929 has subsequently issued as U.S. Patent No. 6,379,383 (the '383 patent"). The '383 patent lists several examples of specific vacuum deposition conditions. See e.g. Examples 1-4 of the '383 patent. Such vacuum deposition conditions disclosed in the '383 patent are remarkably different than Whithcer, i.e. substrate temperature between about 300 and 110 degrees and bias voltage between -1000 and +1000 volts for sputtering. The '383 patent, col. 7, lines 13-15. Whitcher does not teach or disclose such vacuum deposition conditions. As such, the present application supports vacuum deposition conditions to minimize (or substantially eliminate) formation of chemical and intra- and inter-granular precipitates in the bulk material of the as deposited crystalline film, and Whitcher fails to anticipate claims 39-53 and 67-74.

Regarding Claim 58, Whitcher does not teach or suggest that the nickel-titanium has a composition of between about 51.5 and about 55.0 atomic percent nickel. Whitcher only teaches that the nitinol source target includes about 55.9% wt. nickel and the balance essentially titanium. Whitcher, Examples 1-5, ¶¶ [0066]-[0074]. As such, Claim 58 is novel in light of Whitcher.

Thus, for the reasons stated above, Applicant submits that pending claims 39-53 and 67-74 are distinguished from the prior art cited and of record.

Summary

Accordingly, Applicants submit that the pending claims are patentably distinct from and over the art cited and of record. Favorable reconsideration of the rejection of the pending claims is solicited.

Any amendments made during the prosecution of this application are intended solely to expedite prosecution of the application and are not to be interpreted as acknowledgement of the validity of any rejection raised earlier in prosecution, nor as acknowledgement that any citation made against the application is material to the patentability of the application prior to amendment.

This Paper is being concurrently filed with a Request for Continued Examination and payment in the amount of $405.00 as the filing fees for the Request for Continued Examination. No additional fees are believed necessitated by the filing of this Paper. Should any such additional fees be required, the Commissioner is hereby authorized to deduct them from Deposit Account No. 18-2000, of which the undersigned is an authorized signatory.

Should the Examiner believe that there are any outstanding matters capable of resolution by a telephone interview, the Examiner is encouraged to telephone the undersigned attorney of record.

Respectfully submitted

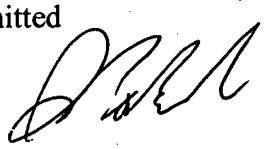

J. Peter Paredes
Reg. No. 57,364

August 17, 2009

ROSENBAUM & ASSOCIATES, P.C.
650 Dundee Road
Suite #380
Northbrook, Illinois 60062
Direct Tel. (847) 770-6016
Fax. (847) 770-6006

Docket No. 6006-015

EXHIBIT A

cientifica

Nanocrystalline Materials

Technology White Papers nr. 4

Paul Holister
Cristina Román Vas
Tim Harper

NANOCRYSTALLINE MATERIALS

Technology White Papers nr. 4

Release Date: October 2003

Published by Científica

Científica, Ltd.
www.cientifica.com

Científica is the world's largest nanotechnology information company. With a global network of partners, the company organizes both scientific and business conferences and provides information and research to thousands of clients worldwide. Científica is the publisher of the Nanotechnology Opportunity Report and TNT Weekly.

Authors

Paul Holister
Cristina Román
Tim Harper

Disclaimer

1. Accuracy of Information.

The information contained in this report has been obtained from sources believed to be reliable. Científica disclaims all warranties as to the accuracy, completeness, or adequacy of such information. The reader assumes sole responsibility for any loss or damage resulting from investment and/or business decisions based on the contents of this report.

2. Views of the authors.

The information contained in this report represents the views of Científica. Científica is solely responsible for the content of this report.

3. Limitation of Liability.

In no event will Científica or any co-author be liable for:

(i) damages of any kind, including without limitation, direct, incidental or consequential damages (including, but not limited to, damages for lost profits) arising out of the use of information contained in this report, or any information provided in this report.

(ii) any claim attributable to errors, omissions or other inaccuracies in this report or interpretations thereof.

Table of contents

Origin of content

The free reports in this series are extracted from the technology reports that make up the Nanotechnology Opportunity Report collection and are designed to offer an introduction to the variety of technologies that fall under the nanotechnology umbrella. The full reports also include 'opportunities' sections, covering the various applications of the technology and their effects on markets, and a list describing the companies involved in the technology.

Introduction

This report covers bulk nanocrystalline materials and coatings. Metals and ceramics (these being metal oxides in the context of this report), both bulk and in coatings, make up most of the content of the report. Both these materials are generally made up of crystals the size of which are measured in micrometers. Reducing the size of the crystals can have quite dramatic effects on the properties of the bulk material, particularly increasing strength.

The creation of nanocrystalline materials is in its infancy. A few companies are starting to commercialize products and significant growth can be expected, penetrating the huge markets for structural materials and coatings. The new products will not be without competition from other materials, especially nanocomposites, but there are markets where these new materials will be the favored choice in the future.

Nanocrystalline materials

Nanostructure and properties

Bulk metals and ceramics and coatings

Metals and ceramics are generally polycrystalline, meaning that they consist of many randomly oriented crystalline regions, or grains. Reducing the size of the grains (also referred to as crystals or domains) in existing materials can have a big impact on bulk material properties. As the grain size in a metal, for example, moves into the nanoscale, an increasing proportion of the atoms in the solid are found on grain boundaries, where they behave differently from those not on boundaries. Their behavior starts to dominate the behavior of the material (at roughly 5 nm, 50% of the volume will be grain boundaries).

Note that a nanocrystalline material need not just be a bulk solid or surface but can be a powder, or nanopowder, thus there is overlap of the use of the terms nanocrystal and nanoparticle for some materials. In general, though, the important properties of nanocrystalline nanoparticles stem from their nanoparticulate nature and will not be considered here (this applies, for example, to nanocrystalline semiconductor quantum dots, where size is the critical property). This report will focus largely on bulk nanocrystalline materials. Nanopowders can, however, be the source material for making nanocrystalline solids and coatings.

It is often stated that as grain sizes move into the nanoscale, metals get stronger and harder (and more brittle) while ceramics become more ductile (malleable). This is an approximation, though, and in fact the reality is more complex and dependent on what part of the nanoscale the grain sizes are in. The approximation stated works, for example, in metals with grain sizes down to about 10 nm, below which a decrease in hardness and strength is seen. In ductile nanocrystalline ceramics, grain sizes are often below this size. The traditional theory behind the change in hardness with grain size is the Hall-Petch relation, which states that hardness increase is inversely proportional to the square root of the grain size (the basis of the effect, put simply, is the limiting of the spread of dislocations, or breaks in the crystal structure, by an increasing number of grain boundaries). This makes for dramatic increases in hardness when going from normal grain sizes to around 10-20 nm.

(Note that grain size is not the only way in which the spread of dislocations can be controlled—creating layered materials can achieve the same effect.)

Other properties of nanocrystalline metals, apart from increased strength and hardness, include higher electrical resistance, increased specific heat capacity, improved thermal expansion properties, lower thermal conductivity and improved magnetic properties.

In ceramics, the increase in ductility when they become nanocrystalline is accompanied by improved toughness (the ability to withstand an impact or applied strain), or reduced brittleness, and improved ability to bond to a metal component. The toughness leads to increased wear resistance (2-4 times that of a traditional ceramic coating) but, somewhat counter-intuitively, grinding and polishing, which is often performed after laying down a ceramic coating, is actually easier with nanocrystalline ceramics.

Increased ductility is especially valuable in ceramics, where brittleness is often a major problem, and superplasticity has been observed in both nanocrystalline metals and ceramics at around 200°C, making for easier forming of materials. The most important impact of increased ductility in ceramics is on ceramic coatings for machinery that resist wear and corrosion. These materials generally fail not because of wear but because of insufficient toughness.

Research into new nanocrystalline ceramic coatings holds promise, with materials such as tungsten-carbide cobalt, chrome oxide and yttria stabilized zirconia being investigated.

The ductility of nanocrystalline ceramics also creates the possibility of drawing them into wires, offering applications based on the superconducting properties of some ceramics.

In metals it is the improved strength that is most sought after, and the increased stiffness can actually be a problem, since ductility is useful not just in manufacturing but also in terms of behavior on impact, an important consideration in cars, for example.

To give an idea of the changes that can be achieved in metals, Rensellaer Polytechnic researchers measured the strength of nanocrystalline copper and found it to be 5 times harder than conventional copper. In fact today's strongest steels have about 10% of the theoretically possible maximum strength.

Loss of ductility in nanocrystalline metals can actually be avoided. This can be achieved by creating a mixture of nanoscale and microscale grain structures. Late in 2002, researchers at Johns Hopkins University managed to create copper that was 75% nanocrystalline with 25% of microcrystalline grains dispersed in the material. It proved to be 5-6 times the strength of normal copper but without any loss in ductility. A ceramic structure with microscale grains embedded in a predominantly nanocrystalline matrix has also been found, by the US's Office of Naval research, to produce the best properties for their aluminum and titanium oxide ceramic coatings.

Note that there are competing approaches to making stronger steels while retaining ductility. Traditional steel has carbon particle inclusions; in 2001, a group at NKK in Japan demonstrated a way of including nanoparticles in the rolling process for steel to make these inclusions smaller, resulting in a new steel that is significantly stronger than existing varieties but with the formability required for uses in creating car engine parts or body components. Toyota, which was involved in the project, is already using the new steel.

Alternatively, crystalline structure can be avoided altogether, by creating amorphous metals, in which there is no particular pattern in the atomic order (glass is a classic example of an amorphous material). In 2001, the US Department of Energy's Idaho National Engineering and Environmental Laboratory developed a spray-on super-hard (and corrosion-resistant) steel amorphous coating that proved remarkably resilient, approaching the best tungsten-carbide coatings in hardness (the application of heat can convert this amorphous coating into a nanocrystalline form), with both strength and hardness reaching 45% of the theoretical maximum. While only coatings have been achieved so far, the hope is to be able to build thick industrial steel sheets out of this material.

Chemical reactions and catalysis

Increased reactivity is also seen in bulk nanocrystalline materials because of increased surface area. This can be useful with respect to direct chemical reactions or in terms of catalytic activity. An example is the lithium tin nanocrystalline alloy made at Brookhaven National Labs early in 2002, in which the 20-30 nm grain size gave improved reactivity, and potentially a more powerful battery. Also, back in 1999, researchers at MIT started creating nanocrystalline high temperature catalysts (used, for example, in the catalytic combustion of natural gas—an area of great interest at the moment) that could be created at lower temperatures than were normally required but would still withstand the high operational temperatures.

Nanostructured cerium ceramics have been shown to offer catalytic activation for sulfur dioxide reduction and carbon monoxide oxidation at significantly lower

temperatures than traditional versions of these catalysts, and they have also shown greater resistance to poisoning (the loss of catalytic reactivity caused by contaminants). Some materials only develop catalytic activity once they become nanostructured, an example being cadmium selenide, which is not normally photocatalytic but becomes so when nanocrystalline, and offers the ability to 'fix' (a term taken from photosynthesis) waste carbon dioxide.

Other nanocrystalline materials of note

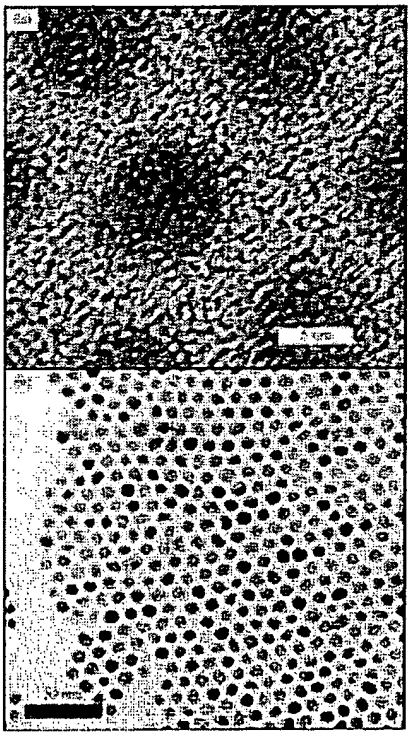

TEM image of (hcp) Co nanocrystals (NCs). Colloidal synthetic methods allow Co NCs to be produced in several distinct crystal polymorphs with varying degrees of crystal perfection. Courtesy of IBM.

Nanocrystalline and nanoporous silicon showed promise in a few research results in 2001 because of their ability to emit light. Nanocrystalline silicon has properties, in addition to electroluminescence (of interest for semiconductor laser applications), such as photoluminescence, thermally-induced acoustic emission, and refractive index changes that can be controlled. The attraction here is the compatibility with silicon-based electronics. Not much research of note has been seen in this area in 2002, however.

Towards the end of 2002, though, nanocrystalline nanoporous silicon was shown to have a property applicable to a very large and dynamic market, that of flat panel displays. Researchers at Tokyo University created nanocrystalline silicon film with a pore structure that varied with depth and in which the electrons could be accelerated to the surface, creating what the researchers called a 'vacuum-less cathode-ray tube'.

Nanocrystalline diamond is another interesting material. Argonne National Laboratory created a film of diamonds that are only 3-5 nm across (each containing around 1000 atoms) by using buckyballs (molecular cages of 60 carbon atoms) as a feedstock. The tiny size changed the electrical properties of the diamond film, when compared with normal diamond films, because of electron transport at grain boundaries (aided by nitrogen), meaning that the diamond can be made to behave as a semiconductor (researchers at CSEM in Switzerland have achieved similar results). The advantage of diamond over silicon is its ability to tolerate extreme environments. It also exhibits much less friction than silicon, and is much stronger, which may be useful in microelectromechanical systems.

The relationship between nanocrystals and magnetism holds the possibility of making stronger permanent magnets. Grain size is already a factor in magnetic materials that

is controlled to achieve desired properties, especially the smallest possible magnetic domains in recording media. Below a certain size a grain is liable to spontaneously switch its magnetic orientation (this relates to the superparamagnetic limit). The latest materials for recording media have elongated grains that allow the total volume of a grain to remain above the limit while presenting a smaller surface profile. Theoretical limits are being approached in this area but in permanent magnets there is still a lot of scope, with some suggesting that 4-5 times the strength of current permanent magnets could be achieved if the ideal grain structure could be attained.

Finally, it should not be forgotten that nature is a master of nanomaterials and nanocrystalline materials are no exception. Many groups are working on borrowing from nature to make nanostructured materials, either by emulating natural processes or by modifying biomaterials directly (for example, by taking the shells of tiny marine organisms, called diatoms, and chemically modifying them). However, natural materials like this are not generally nanocrystalline in the sense of having multiple nanoscale crystal domains, but tend to be instead a more globally structured crystalline form. An example of some work done in this area, which does indeed produce a nanocrystalline material as an approximation of the material that nature produces, is research done on hydroxyapatite by MIT.

Hydroxyapatite is the main mineral component of bone and synthetic versions tend not to be anywhere near as strong as natural ones. MIT's version was built by coalescing nanoscale particles into a solid that was much closer to the strength of bone than traditional synthetic versions.

Production techniques

Materials can be made nanocrystalline using quite a wide variety of techniques.

For coatings, new techniques, such as pulsed laser deposition or electrodeposition, or variants of chemical vapor deposition techniques, have been developed that can coat a surface with nanocrystalline metals, semiconductors and other materials.

Thermal spraying is an increasingly popular way of converting the new generation of nanopowders into nanocrystalline coatings—heat is used to partially melt the powders so that they fuse when they form the coating. Varying the amount of melting can lead to different structures. A variation of this technique, using a plasma (a hot, ionized gas) into which nanoparticle agglomerates are fed, is used to produce the ceramic coating used by the US Navy (previously mentioned) and other ceramic coatings. The nanostructure is created by retaining some of the original nanoparticle structures (thus only limited melting can be allowed), or by mixing nanoparticles with different melting temperatures, or by allowing the nanostructure to form in the applied coat through the combining of non-miscible materials. This approach was used to achieve the useful mixture of nanoscale and microscale grains.

Electrodeposition is an old coating process but has been successfully customized to produce coatings with grain sizes down to 5 nm. It is a commercially attractive

process because it can be carried out at room temperature and can be used for large-scale production.

To create bulk materials that are nanostructured in three dimensions, powder compaction, crystallization of initially amorphous material, and severe plastic deformation processing are the leading methods but approaches such as electrodeposition have also been used.

Powder compaction methods involve first producing nanoscale particles which are subsequently fused together using combinations of pressure and heat. Nanoparticles can be made to partially melt and fuse at temperatures below the normal melting point of a material. These methods have been limited by the challenge of controlling contamination or oxidation of the high surface area particles that are the raw material, and the resulting materials also tend to be porous, but the methods offer the advantage of being able to combine different particles to create nanocomposites.

Severe plastic deformation (SPD) processing techniques are applicable mainly to metals. These methods all take advantage of the ability of the crystals within metals to subdivide into domains as small as 20 nanometers when they are subjected to large shearing strains while under high pressure, though crystal sizes a little below 100 nm are more common. The strain can be applied in a number of ways, such as extrusion, bending or twisting, or rolling.

SPD approaches have the advantage over powder methods for bulk solids that they can create nanocrystalline materials with minimal porosity and contamination.

SPD is scalable and is thus being pursued for commercialization. However, there is an inevitable additional cost and sometimes the resulting material contains unwanted stresses.

The super-strong but ductile copper made at Johns Hopkins University used a variant of deformation processes. Rolling created the nanostructure and subsequent annealing (a process involving heating to below the melting temperature, usually used to relieve stresses) led to the formation of some micrometer-sized grains.

Purdue University researchers made a serendipitous discovery in mid 2002 that seems obvious in retrospect. Shavings from working metals are, of course, subjected to great stress. The Purdue researchers discovered that the materials are often nanocrystalline as a result, offering the possibility of making nanocrystalline bulk materials out of waste that would normally be melted down and recycled.

Crystallization of amorphous materials can produce the finest scale nanostructures, but is limited to materials that can be first put into an amorphous state. However, approaches such as sol gel allow the creation of a wide variety of materials with a very well-controlled nanostructure (if not necessarily nanocrystalline) and have been used to make ultra-non-stick ceramic coatings.

The lithium tin nanocrystalline alloy made at Brookhaven National Labs, which was used as a high-performance electrode, was created using a rather original technique, reacting lithium hydride with tin oxide, but with more of the former than was needed to react fully. This produced a lithium tin alloy with lithium oxide left over. Repeatedly adding and removing hydrogen produced a nanocomposite with grain sizes of 20-30 nm. The researchers say that other elements that form stable metal hydrides could be used to make nanocomposite materials with this method, with potential applications not just in batteries but also in catalysis.

EXHIBIT B

Min Invas Ther & Allied Technol 2000: 9(1) 107–118

Optimisation of processing and properties of medical grade Nitinol wire

A.R. Pelton[1], J. DiCello[1] and S. Miyazaki[2]

[1]Cordis Corporation – Nitinol Devices and Components, Westinghouse Drive, Fremont CA, USA; and [2]Institute of Materials Science, University of Tsukuba, Ibaraki, Japan

Summary

The purpose of this paper is to review the current processing and resultant properties of standard Nitinol wire for guide-wire applications. Optimised Ti-50.8at%Ni wire was manufactured according to industry standards by precise control of the composition, cold work and continuous strain-age annealing. Mechanical properties of this wire are reported from −100°C to 200°C to demonstrate the effects of test temperature. Within the 'superelastic window' the plateau stresses are linearly related to test temperature. Additional ageing treatments can be used as a tool to fine-tune transformation temperatures and mechanical properties. A review of the fatigue properties of thermomechanically-treated Nitinol wire shows that they are affected by test temperature, stress and strain.

Keywords

Nitinol, shape-memory, superelasticity, mechanical properties, ageing, fatigue

Introduction

The growth in the use of Nitinol in the medical industries has exploded over the past 10 years. Patients and care-providers have encouraged the transition from traditional open-surgical procedures that require long hospital stays, to less-invasive techniques, which are often performed in out-patient facilities [1]. This demand for minimally-invasive procedures has required novel instrumentation and implants to be designed by engineers and physicians. An increasing number of these devices use Nitinol as the critical component. Examples of these medical applications are richly illustrated in companion articles in this journal [2,3], and range from endoscopic instruments to implants, such as stents and filters. It is interesting that the majority of these devices depend on mechanical superelastic behaviour, which is a significant departure from the original thermal shape-memory industrial uses of Nitinol.

Since the 'discovery' of the shape-memory effect in TiNi alloys in the 1960s, metallurgists have investigated methods to control transformation temperatures and mechanical properties through alloying additions, improved melting practices and thermomechanical processing (see, for example, References 4 and 5). The production of many thousands of kilometers of wire for such diverse products as cellular telephone antennae, eyeglass frame components, guidewires, undergarment supports and orthodontic archwires profoundly influenced the acceptance of Nitinol in the marketplace. These commercial opportunities have allowed Nitinol suppliers to focus on improving

Correspondence: A. Pelton, *Cordis Corporation – Nitinol Devices and Components, 47533 Westinghouse Drive, Fremont CA 94539, USA.*

processes for a few standard alloys, rather than pursuing a myriad of 'boutique alloys' with niche applications. The composition and processes have been refined so that, for example, the transformation temperature in final products is routinely controlled to within ± 3°C. More recently, the availability of seamless tubing and sheet have provided designers with additional tools to solve engineering problems. Furthermore, microfabrication techniques, such as laser machining [6] and photoetching [7], have also contributed to the increase in the number of miniature devices made from Nitinol.

Accordingly, Nitinol properties have become very predictable, which is a basic requirement of design engineers. As the Nitinol industry has matured over the past two decades, terms such as 'shape-memory', 'superelasticity', 'recovery forces', 'plateau stresses', and 'transformation temperatures' are now recognised by more than just a select few metallurgical specialists. Although design engineers have a good understanding of the basic properties of the alloys, they still have many good questions. Typically these include:

- Are the mechanical properties constant over a wide range of temperatures?
- Can we adjust the transformation temperature without modifying the mechanical properties?
- Do the shape-memory and superelastic properties imply that Nitinol has an infinite fatigue life?

The purpose of this article is to address these questions by reviewing the processing and resultant properties of Ti-50.8at%Ni wire that has been manufactured for medical guide-wire applications. Furthermore, this article will focus on the effects of standard continuous thermomechanical processes, rather than long-term 'batch' processing, which was more common in the 1970s and 80s.

Processing

Optimisation of the superelastic properties of Nitinol for a specific product is achieved through a combination of cold work and heat treatment. The first step in optimising the thermomechanical treatments of wire and tubing products is to draw the material through a series of dies, to achieve 30–50% reduction in cross-sectional area [8]. Past methods have employed a long-term batch annealing process but, to attain a more uniform product, continuous strand strain annealing is the most effective method. With this method, the Nitinol wire is under constant strain during the annealing process. Continuous 'strain annealing' ensures that the entire spool will be processed with the identical thermomechanical treatment, resulting in a product with uniform properties from end to end.

Figure 1 shows a typical continuous-strand strain straightening process line.

Continuous-strand straightening usually occurs in a temperature range of 450–550°C under a stress of 35–100 MPa. As the wire moves into the heat zone it will initially want to shrink in length and grow in diameter, due to the shape-memory effect not suppressed by the cold work of the drawing process (springback). The wire temperature quickly increases, its strength will drop and the applied strain will straighten the wire and, depending on the strain, reduce the wire diameter slightly. In the continuous process it is difficult to measure the active strains during straightening as they occur inside the furnace. However, the following vertical straightening example can help define the strains operating during the continuous process.

During vertical straightening of discrete lengths of wire, the wire is heated via electrical resistance and is therefore exposed to make visible measurements. As a 1.5 mm diameter wire was being electrically straightened, it showed a maximum springback of 1.2% during heating and a 2.4% extension strain at the end of the straightening cycle. Similar strains would be expected with the continuous-strain straightening method.

Straightness, mechanical properties and the active A_f are all affected by the speed and temperature parameters of the straightening process. As with all thermally-activated processes, time at temperature controls the final properties of the wire. More time at temperature softens the wire and moves its mechanical properties toward a fully annealed product, while short times leave the material closer to the high strength cold-worked state. To optimise the superelastic properties, a balance must be developed between these two extremes. The requirements of

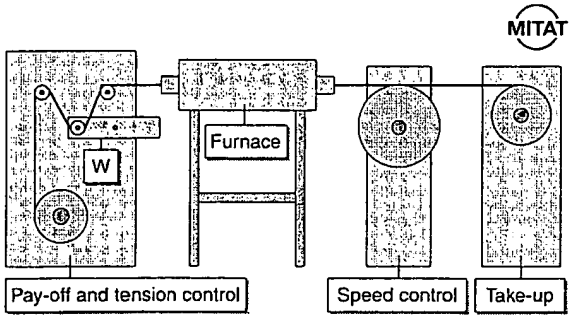

Figure 1. Schematic diagram of a continuous strand annealing equipment for optimised production of Nitinol superelastic wire.

the final product will help define the process parameters. A high torqueable guide-wire may require slower speeds than a high strength wire that has a table-roll straightness requirement. Additional speed and temperature adjustments may be necessary to meet any active A_f requirements (see discussion below) as well.

Properties

In this section we will consider the methods of characterising the thermal and mechanical properties of thermomechanically-processed wire. The focus will be on products that are superelastic between room temperature and body temperature. We will document the mechanical properties from −100°C to 200°C, to illustrate how test temperature affects performance. Furthermore, since many wire and tubing products are given additional thermal shape-setting, we will establish the effects of ageing time and temperature treatments on transformation and mechanical properties. Finally, since many Nitinol medical devices are used in (human) fatigue environments, we will discuss the influence of strain amplitude and test temperature on bending fatigue behaviour.

Transformation temperatures

Harrison [9] cataloged >20 techniques that have been used to measure the changes associated with the shape-memory transformation. Two of the most fundamental ways to determine the **qualitative** transformation temperature involve sound and feel. Even a novice can distinguish between the 'ping' from austenite and 'thud' from martensite when dropped on the floor. Although this is not a highly quantitative means to measure transformation temperatures, it has been used to sort alloys quickly without sophisticated equipment. Another qualitative method is to feel the alloy. Martensite 'feels' rubbery when bent, whereas austenite feels 'springy'.

These two simple examples cited above illustrate that the martensitic transformation affects a variety of properties. However, Harrison [9] offered the sage advice that the chosen measurement technique should parallel the actual function of the product. For example, many medical customers request certification of the A_f temperature to ensure that the product is austenitic above a certain application temperature. These customers generally specify that the measurements are obtained by either differential scanning calorimetry (DSC) or free recovery ('active') techniques. DSC measures the heat released and absorbed during the martensitic (exothermic) and austenitic (endothermic) transformations, respectively [10, 11]. Free recovery, however, is by far the most simple and often the most useful method to measure A_f. This technique only requires the following steps, which simulate a shape-memory cycle:

- cool to a low temperature (for example in a cooled alcohol bath);
- bend the sample to a prescribed strain (2–3%);
- watch and record the temperature at which the sample returns to its original shape when heated: this is defined as the A_f temperature.

Free recovery can also be instrumented in order to obtain a permanent record of the results [12, 13]. Both of the above techniques have the benefit that they are straightforward to conduct, amenable to use for small specimens, require minimal sample preparation (especially free recovery) and are reproducible.

Figure 2 compares the DSC thermogram and instrumented free-recovery measurements from the same wire. The DSC records the heat flow during both cooling and heating, whereas free recovery records the deflection recovery only during heating. The key transformation temperatures, martensite start (M_s), martensite finish (M_f), austenite start (A_s) and austenite finish (A_f), are marked as appropriate on both charts. Also included are atomic models of the austenite (cubic structure) and martensite (monoclinic structure) to help the reader visualise the transformations.

Note that the DSC graph shows an R-phase peak during cooling from a high temperature. Although an in-depth discussion of the R-phase is beyond the scope of this paper, it is important to point out that the R-phase is another shear transition in competition

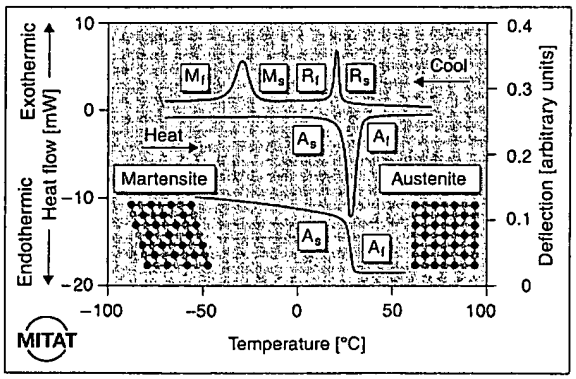

Figure 2. Differential scanning calorimetry and free recovery of the same processed wire. Note that upon cooling the wire transforms to R-phase prior to the martensitic transformation. Upon heating, both techniques provide similar A_s and A_f temperatures as the (monoclinic) martensite transforms to the (cubic) austenite.

with martensite [14]. In the case shown in Figure 2, the R-phase forms around room temperature. With further cooling, the martensite transformation begins at about −23°C (M_s) and is fully martensitic below −38°C (M_f). When the sample is reheated, the reverse transformation begins at about 22°C (A_s) and finishes at an A_f of 32°C. Note that there is a wide hysteresis between the M_f and A_f, which is characteristic of shape-memory alloys. The origin of the hysteresis is attributed to microscopic internal friction effects [15]. The A_s (24°C) and A_f (32°C) data from the free recovery method are nearly identical to those from DSC.

Mechanical properties

Based on the transformation behaviour shown in Figure 2, the wire should be fully austenitic above 32°C. However, an important characteristic of shape-memory alloys is that stress can trigger the martensitic transformation at temperatures above A_f (the 'thermoelastic' effect [15]). From a thermodynamic viewpoint, this means that it is easier (lower free energy) for the wire to create martensite in response to the applied stress than to deform plastically (dislocation formation) [15,16]. Stress-induced martensitic transformations can be easily understood by considering Figure 3 [17]. This diagram compares atomic motions in response to an applied stress by traditional Hookian elastic (top) and transformational superelastic (bottom). For Hookian elasticity, which represents conventional materials, such as stainless steel, the atomic bonds 'stretch' up to about 0.5% before plasticity occurs. In contrast, the austenitic structure depicted on the bottom left structure transforms into martensite with applied stress. As the magnitude of the stress increases from left to right, the amount of martensite increases. Up to 10% strain can be accommodated by stress-induced martensitic transformations. The martensitic structure formed by superelasticity is identical to that formed through the shape-memory process, as illustrated in Figure 2.

Figure 4 is a schematic stress–strain curve that corresponds to this model of transformational superelasticity. When the wire is pulled beyond its Hookian elastic limit (approximately 1.5% strain in Nitinol), there is an apparent 'yield' at a critical stress. Atomistically, this is represented by the onset of martensitic transformation, as shown in the second diagram in Figure 3. The wire can be further stretched at a relatively constant stress along the 'loading plateau' until the entire structure has transformed into martensite. As the stress is removed, the martensite immediately recovers elastically (linear unloading) and then begins to revert back to austenite on the 'unloading plateau'. The ability of the material to return to its original shape when the stress is released is an important attribute for many products,

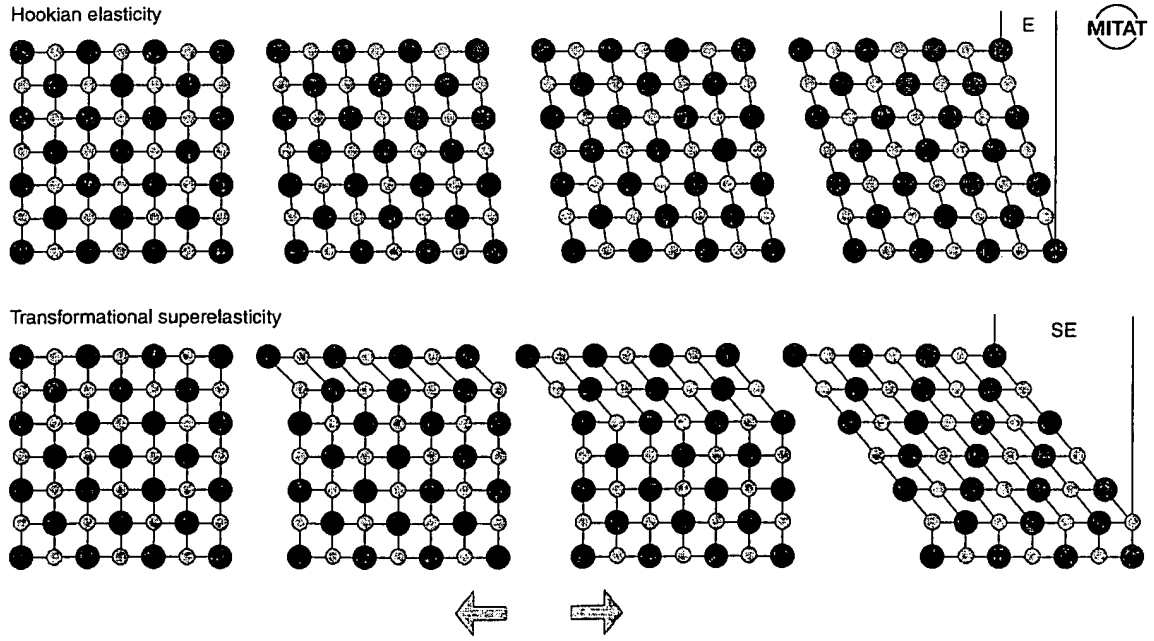

Figure 3. Schematic representation of the atomic motions associated with Hookian elasticity observed in conventional materials and transformational superelasticity of Nitinol. (From Stöckel and Yu, Ref. 17.)

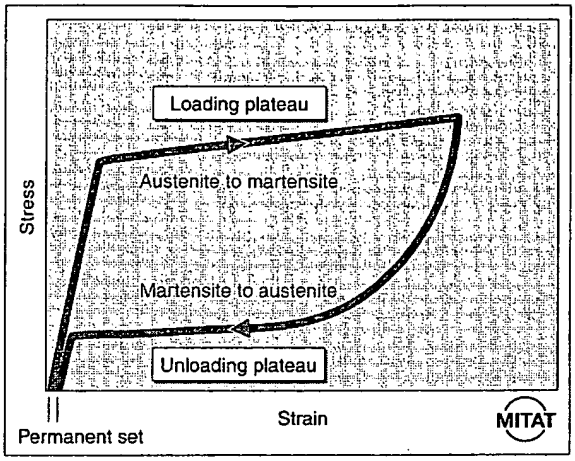

Figure 4. Schematic stress–strain curve of superelastic Nitinol. There is a transformation from austenite to martensite that begins at the apparent yield stress. The plateau stress remains nearly constant with increasing strain as the amount of martensite increases. Upon unloading, the martensite reverts to austenite along the unloading plateau. The 'permanent set' measures any residual strain.

such as guide-wires, to minimise kinking. Any residual strain is caused by an accumulation of plastic strain and is measured by the 'permanent set', as shown on the figure. Note that the stress–strain curve exhibits a stress hysteresis that, similar to the thermal hysteresis discussed above, is due to microstructural frictional effects. The magnitude of the stress hysteresis plays an important role in the design of many Nitinol applications, such as Nitinol eyeglass frames. A high loading stress is required to resist easy bending of the frame, whereas the unloading stress should be low so that the temples exert a gentle pressure against the head. Stöckel [2] discusses other examples of this 'biased stiffness' property.

Effects of test temperature

The tensile curves shown in Figure 5 illustrate that the mechanical behaviour of Nitinol varies greatly from −100°C to 150°C. In these tests, wires with an A_s of −22°C and A_f of 11°C were pulled to 6% strain, unloaded to zero stress and were then pulled to failure. At the lowest test temperatures, the wires are martensitic and the high residual strains are fully recovered by heating above A_f (the shape-memory effect). From about 0°C to 100°C the tensile curves exhibit superelastic 'flags', and we note that it becomes more difficult to stress-induce martensite as the test temperature increases. Along with the increase in the plateau stresses, the permanent set also increases with temperature. The tensile behaviour at 100°C, with a high permanent set, but a well-defined unloading curve, indicates that deformation is accommodated by a combination of stress-induced martensite and conventional plasticity. Above 150°C, however, the wire deforms by plastic mechanisms rather than martensitic transformations, which results in a linear unloading curve. The temperature where it is too difficult to stress-induce martensite is defined as M_d; in the present case, M_d is between 100°C and 150°C.

The effects of test temperature on the tensile curves shown in Figure 5 may be further analysed by considering each of the key attributes. For example, Figure 6 shows the temperature dependence of the permanent set from these wires after unloading from 6% strain. At lower temperatures, the unresolved strain is due to deformation of the martensite, and can be recovered by heating above A_f. The residual strain is nearly zero between 0°C and 60°C, which defines the superelastic 'window' for this alloy. As noted above, the non-recoverable plastic strain is about 1 % at 100°C and then increases to about 3 % at 150°C. Many medical applications require superelastic behaviour between room temperature and body temperature. Therefore, this 60°C window is perfectly centered about the intended application range.

Figure 7 shows the effects of test temperature on the loading, unloading and ultimate tensile stress. We see that there is a linear relationship between plateau stress and temperature between about 0°C and 60°C for the unloading plateau and up to 150°C for the loading plateau. These variations in plateau stress follow the Clausius–Clapeyron relationship for a first-order transformation [16]:

$$\frac{d\sigma}{dT} = \frac{-\Delta H}{T\varepsilon_0}$$

Where $d\sigma$ is the change in plateau stress, T is the test temperature, ΔH is the latent heat of transformation (obtained from DSC measurements), and ε_0 is the transformational strain. ΔH and ε_0 are controlled by the crystallography of the transformation and can be considered constants. The right side of the equation therefore defines the 'stress rate' for the stress-induced transformations. For the present case, the stress rate is 6.1 MPa°C^{-1}, which is within the typical range of 3–20 MPa°C^{-1} for Nitinol alloys [18]. The consequence of this relationship is that the mechanical properties of Ti–Ni alloys depend directly on the transformation temperature and test temperature.

The ultimate tensile stress (UTS) gradually decreases from approximately −100°C to 150°C, with a slight minimum at 150°C. The UTS and plateau

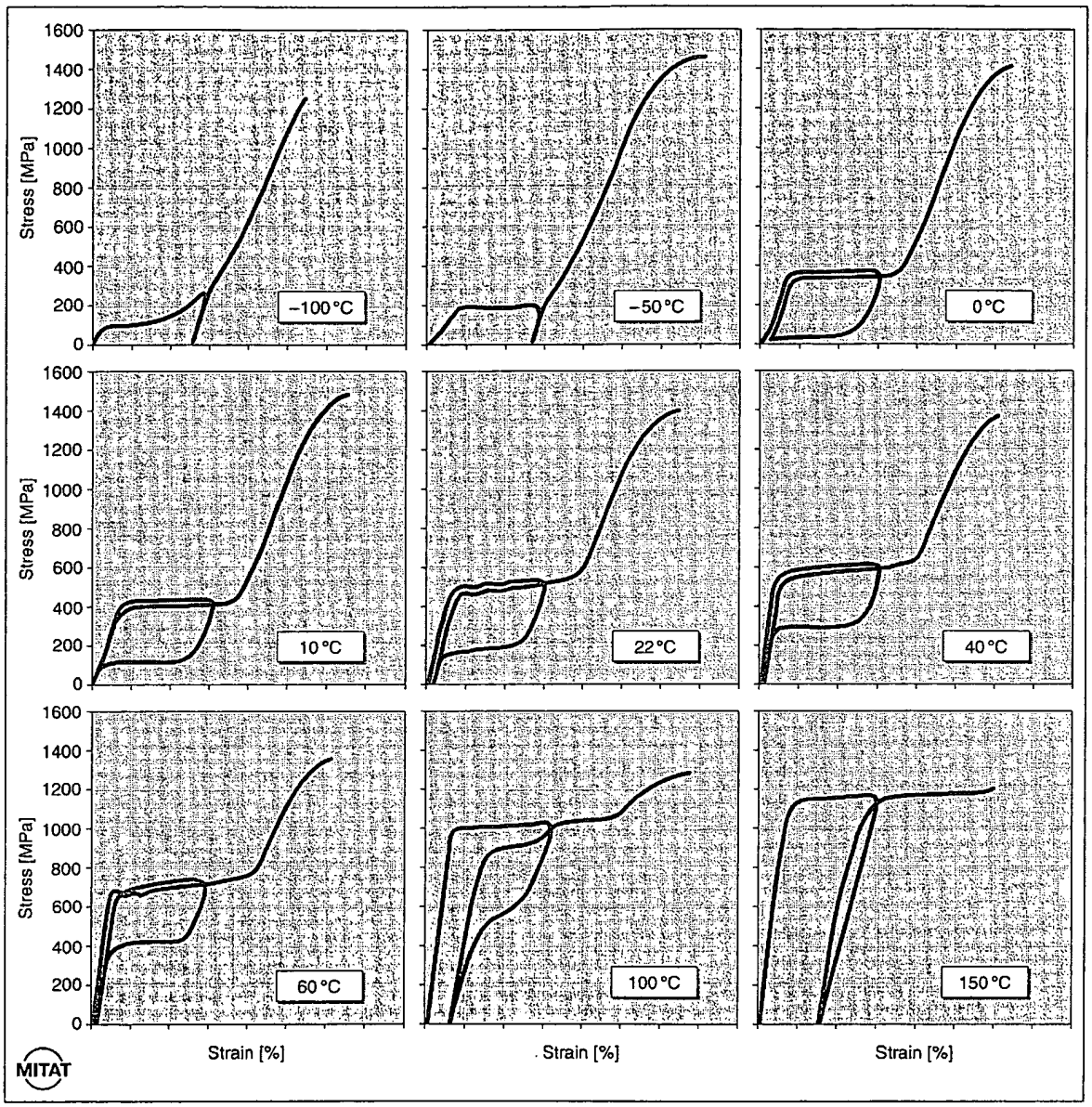

Figure 5. Effect of test temperature on the mechanical behaviour of Nitinol wire. Note that there is a systematic increase in the loading and unloading plateau stresses with increasing test temperature. Below 0°C, the structure is martensite and, above 150°C, the graph shows conventional deformation of the austenite. The intermediate temperatures all show classic transformational superelasticity.

stress converge above this temperature, which is a further indication that M_d is near this temperature. In Figure 8, we see that the elongation is fairly constant up to about 150°C and then drops at the higher temperatures. The combination of the low ductility and high stresses above 150°C may indicate a toughness minimum for this material.

Effects of ageing heat treatments

Several investigators have shown that optimal superelastic performance can be achieved in Nitinol alloys that have a combination of cold work and ageing heat treatments [18, 19]. Precise control of these thermomechanical treatments can lead to reproducible mechanical properties and transformation temperatures. TiNi alloys with 50.8% Ni respond well to ageing heat treatments to 'tune in' the

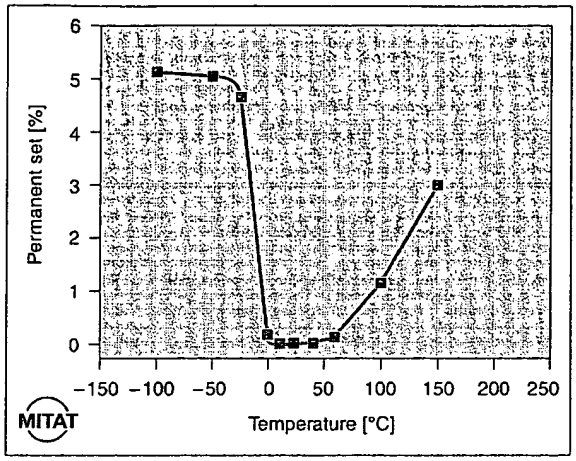

Figure 6. Effect of test temperature on permanent set is shown from the data in Figure 5. The 'superelastic window' extends from approximately 0°C to 60°C, where there is minimal residual strain after unloading from 6 % strain. Below 0°C, the strain can be recovered by heating above A_f = 11°C (the shape memory effect) and at higher temperatures the residual strain is due to plasticity.

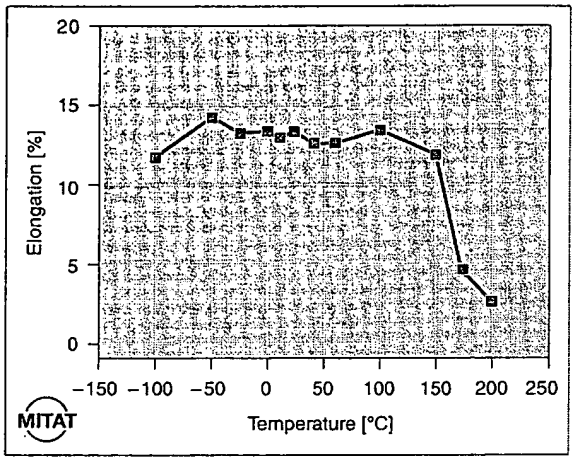

Figure 8. Effect of test temperature on elongation is shown from the data in Figure 5. The elongation does not vary much with temperature up to approximately 150°C. The drop in ductility at the high temperatures may signify a toughness minimum.

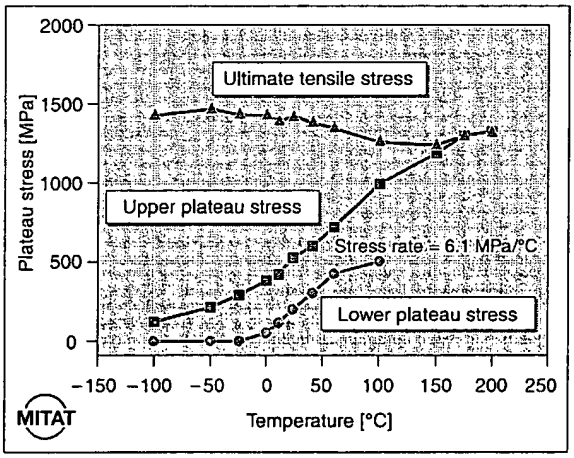

Figure 7. Effect of test temperature on plateau and tensile stresses is shown from the data in Figure 5. Note that there is a linear relationship between plateau stress and test temperature from about 0°C to 100°C with a slope, or stress rate of 6.1 MPa/°C^{-1}. The ultimate tensile stress shows a gradual decrease with increasing temperature with a minimum at the M_d of 150°C.

desired properties. Nishida *et al.* [20] established the effects of ageing time and temperature on the Ti-Ni precipitation reactions in Ti-51%Ni alloys by metallographic methods. They observed precipitation sequence of $Ti_{11}Ni_{14}$ – Ti_2Ni_3 – $TiNi_3$ in the TiNi matrix at temperatures between 500°C and 800°C and for times up to 10 000 h and presented the data in a time–temperature–transformation (TTT) diagram. Their work gave great insight into the metallurgical tool of controlling precipitation reactions in Nitinol alloys.

Clearly, however, the times investigated by Nishida *et al.* [20] are significantly longer than can be tolerated in a production environment. Therefore, straight wires from the previous section were aged between 300°C and 550°C for 2 – 180 min, to characterise the effects on transformation temperature and mechanical properties. Figure 9 illustrates these effects on the A_f temperature. We note that the transformation temperature does not change significantly at 300°C. Also, at 500°C, the A_f increases slightly at short times, but does not increase rapidly. The intermediate temperatures, namely 350 – 450°C, have a greater impact on the transformation temperature. At the highest ageing temperature, 550°C, there is an initial decrease in A_f and then a rapid increase. Admittedly, these trends of temperature and time on the A_f may appear counter-intuitive. However, more clarity is gained by grouping the time–temperature conditions to obtain common A_f temperatures. Figure 10 is such a TTT diagram, where each 'c-curve' represents the loci of constant A_f. This figure illustrates that there is a maximum in the precipitation reaction at about 425°C; i.e., the A_f increases most rapidly after heat treatments at 425°C. For example, the A_f increases from 11°C in the as-straightened wire, to 30°C after ageing for only 10 min. To reach the same 30°C A_f at 500°C takes about 60 min and at 300°C the time exceeds 180 min.

It is certainly beyond the scope of this article to review the metallurgy of precipitation reactions. However, the shape of these curves can be understood

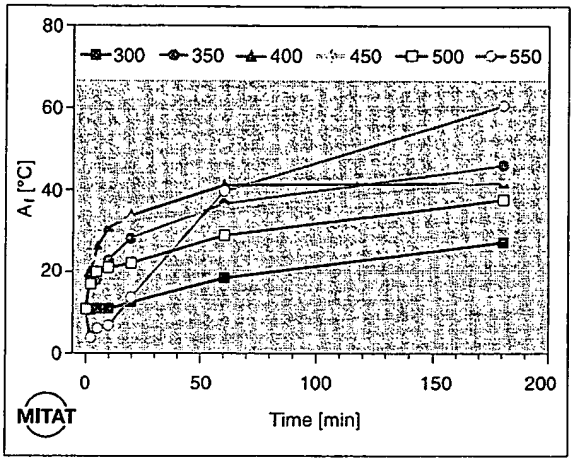

Figure 9. Effect of ageing temperature and time on the transformation temperature of Ti-50.8% Nitinol wire with a starting A_f temperature of 11°C are shown. Note that all of the ageing temperatures tend to increase the transformation temperature, although at 550°C there is an initial decrease.

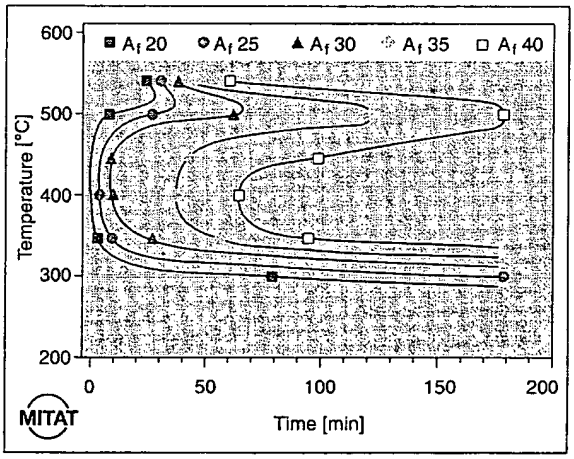

Figure 10. Effect of ageing temperature and time on the transformation temperature of Ti-50.8% Nitinol wire with a starting A_f temperature of 11°C are shown. The data from Figure 9 are re-plotted to illustrate the conventional time–temperature–transformation (TTT) diagram. Note that the maximum precipitation rate is about 400°C. Between 500°C and 550°C the precipitates dissolve and tend to lower the A_f. A new precipitate forms at 550°C (see text for more details).

by briefly exploring two factors that govern diffusional nucleation and growth of precipitates [21]. At high temperatures, there is sufficient thermal energy to permit rapid diffusion of Ni and Ti atoms in the matrix. However, it becomes more difficult for the atoms to form a precipitate nucleus as the temperature increases. At lower temperatures, however, just the opposite situation occurs: here we have high nucleation rates, but low diffusion rates. These two processes are optimised at the intermediate temperatures (350 – 450°C) to achieve maximum precipitation rates. The A_f change, therefore, is due to relative Ni and Ti atom diffusion, where the Ni atoms congregate in the precipitates and the Ti atoms move to the TiNi matrix phase. As the matrix becomes enriched in Ti, the transformation temperature increases, as expected from the relationship of composition to transformation temperature [22]. Although the overall composition of the material remains Ti–50.8% Ni, localised shifts of composition can affect the transformation temperatures.

The trends in the TTT curves indicate that a single precipitation reaction ($Ti_{11}Ni_{14}$) occurs in the temperature range 300–500°C. Between 500°C and 550°C, however, there are 'cusps' in the A_f curves. Above 500°C, the $Ti_{11}Ni_{14}$ precipitates dissolve and there is a corresponding **decrease** in the transformation temperature, as the Ni atoms diffuse back into the matrix. At 550°C the Ti_2Ni_3 phase precipitates require an even greater amount of Ni to diffuse away from the matrix. Precipitation of this phase, therefore, will again increase the A_f, but at a different reaction rate than for $Ti_{11}Ni_{14}$. These findings are consistent with Miyazaki's microstructural study of Ti-50.6%Ni alloys after ageing for 60 min at 400°C, 500°C and 600°C [19]. His results demonstrate that the maximum density of $Ti_{11}Ni_{14}$ precipitates is obtained at 400°C.

The effects of the ageing treatments on the loading plateau stress are shown in Figure 11. Since the wire was 'strain-aged' during the initial processing, these additional ageing treatments do not increase the loading plateau. Ageing temperatures in the 300–500°C range systematically decrease the loading plateau, as we would expect with the increase in A_f temperature. At 550°C, there is an initial decrease in loading plateau stress and then a more rapid decrease as ageing and annealing processes occur. The effects of ageing on the UTS are more interesting, as seen in Figure 12. Here the ageing treatments between 300°C and 450°C increase the UTS. This illustrates that the $Ti_{11}Ni_{14}$ precipitates are effective barriers to dislocation motion. Although we know that precipitates form during ageing at 500°C and 550°C, there is a dramatic decrease in UTS, especially at 550°C. The decrease in plateau and tensile stress at 500°C and 550°C illustrates that this is an effective temperature range for annealing (dislocation annihilation).

The above ageing discussion points out that the transformation temperature can be readily adjusted by

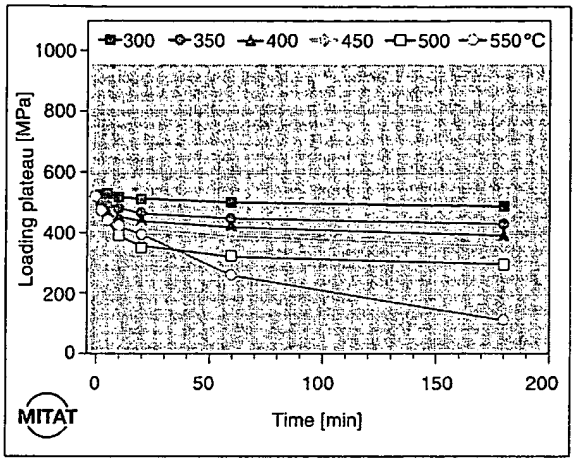

Figure 11. The effect of time and temperature on the loading plateau of aged Ti-50.8% Nitinol alloy. These stress data correspond to the A_f temperatures shown in Figures 9 and 10. There is a systematic decrease in plateau stress with increasing temperature. There is a more dramatic effect at 550°C.

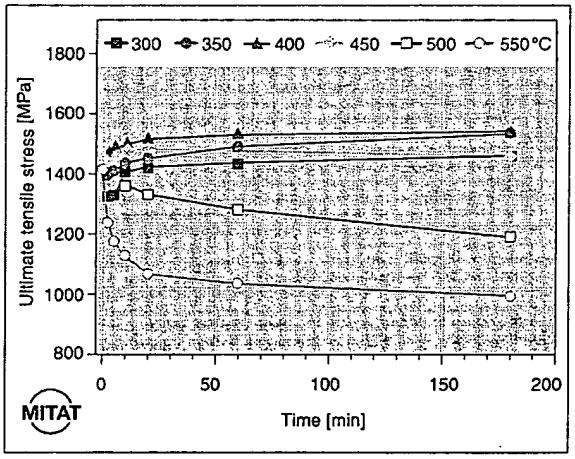

Figure 12. The effect of time and temperature on the ultimate tensile stress. Ageing temperatures between 350°C and 450°C tend to increase the tensile strength due to precipitation hardening. At 500°C and 550°C, the annealing effects dominate and lower the strength.

selecting an appropriate time and temperature. Higher A_f temperatures are achieved by ageing in the 300 – 500°C range. Additionally, the A_f can be lowered by short ageing times between 500 and 550°C.

Fatigue properties

Fatigue life is a major concern for biomedical implant applications. For example, the US FDA requires proof of fatigue resistance of 10 years (400 million cycles) in simulated body environment for intravascular stents [23]. Pedersen *et al.* [24] measured 6% average diametral strain in proximal aorta at 100 mmHg pressure differential. Therefore, an implanted device could be exposed to pulsatile strains as high as 6%. The actual mean strain that the implant is subjected to depends on material and design factors. However, whether the stent is manufactured using woven wire, etched sheet, or laser-cut tubing, the strut sections undergo cyclic bending deformation. Although several papers have reported on the fatigue properties of Ti–Ni alloy plates and bars [25] under tension–compression conditions, only a few recent papers have been published on the fatigue life of Ti–Ni wires [26, 27]. Furthermore, many Nitinol products are tested under accelerated pulsatile conditions that allow only periodic observations to ensure that the devices have not fractured (for example, see Reference 28). A logical approach, however may be to supplement these 'submission tests' with more fundamental bend–fatigue studies on wires or stent elements to aid in the design phase. The purpose of the present section, therefore, is to review the effects of strain amplitude, stress and test temperature on the fatigue life of binary Ti–Ni alloy wires.

Miyazaki *et al.* tested cold-worked and aged Ti-50.0at%Ni [27] and Ti-50.9at%Ni [28] wires in a rotary-bend apparatus. The specimens were fixed in a bent shape with a suitable radius of curvature to induce a desired strain at the specimen surface at specified temperatures above and below A_f. Figure 13 shows the (outer fibre) strain amplitude (ε_a) versus number of rotations to fracture (N_f) relationship at each test temperature for the two alloys. The upper diagram shows three curves for the Ti-50.9at%Ni alloy and the data for the Ti-50.0at%Ni alloy is in the lower diagram. Both alloys show a general trend of increasing fatigue life with decreasing test temperature in the highest and intermediate strain-amplitude regions. In the higher Ti alloy the fatigue-endurance limit increases with decreasing temperature below A_f. The fatigue limit is insensitive to temperature for the Ti-50.0at%Ni alloy above A_f and for all conditions for the Ti-50.9at%Ni.

Miyazaki *et al.* [27] carefully studied the details of tensile stress–strain curves, to gain insight into the fundamental mechanisms that influence fatigue behaviour and give rise to the differences observed in Figure 13. They measured the proportional stress limit (σ_{pr}) and the critical stress to induce the martensitic transformation (σ_M) and corresponding strains, as schematically illustrated in Figure 14. Below the proportional limit strain (ε_{pr}) there is pure elastic deformation, whereas between ε_{pr} and the elastic limit strain (ε_e) there is an elastic deformation, including microscopic local twinning or microscopic

local stress-induced transformation. The authors further note that the difference between ε_{pr} and ε_e is small below A_f and increases with increasing temperature above A_f, especially for the Ti-50.0at%Ni alloy.

The differences in the fatigue behaviour of these wires can be further understood by considering the mechanisms of the phase deformation. Above A_f, deformation occurs by stress-induced martensite, which is the most severe among the modes tested. Between A_s and A_f deformation is partial stress-induced martensite and partial twinning of the martensite. Testing just below A_s gives rise to a different mode of deformation. In this case, the first cycle is stress-induced martensite, followed by twinning of the martensite. At the lowest test temperatures, deformation is accommodated by martensitic twinning. It is interesting that the fatigue-crack propagation behaviour of Ti–Ni alloys is also differentiated by the details of the deformation mode. Dauskardt *et al.* [29] observed that fatigue-crack growth rates were much slower in fully martensitic Ti–Ni alloys than in alloys that undergo a stress-induced transformation.

Since Nitinol alloys perform better under strain control than under load control, most fatigue studies plot fatigue life as a function of strain, as shown in Figure 13. However, deformation stresses also affect fatigue life, so it is also necessary to compare the fatigue behaviour in terms of stress. In particular, the stress endurance limit for the alloys can be related to the test temperature. For example, the Ti-50.9at%Ni fatigue data from Figure 13 are re-plotted in Figure 15 as a function of stress. The stress endurance limits from both alloys show a linear relationship when

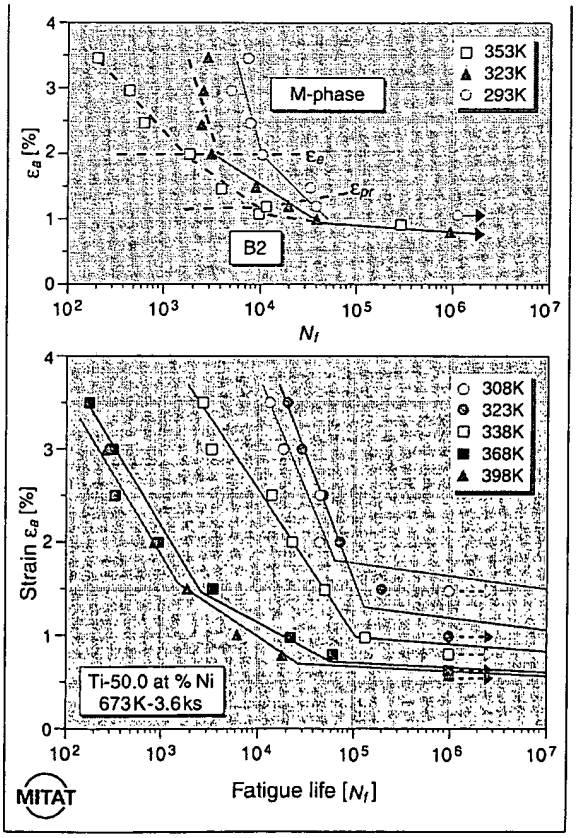

Figure 13. This figure shows the effect of applied strain on the rotary bending fatigue life for Ti-50.9at%Ni (top) and Ti-50.0at%Ni (bottom) alloys at various test temperatures. The endurance limit tends to increase with decreasing test temperature. (After Miyazaki *et al.* Refs 26 and 27.)

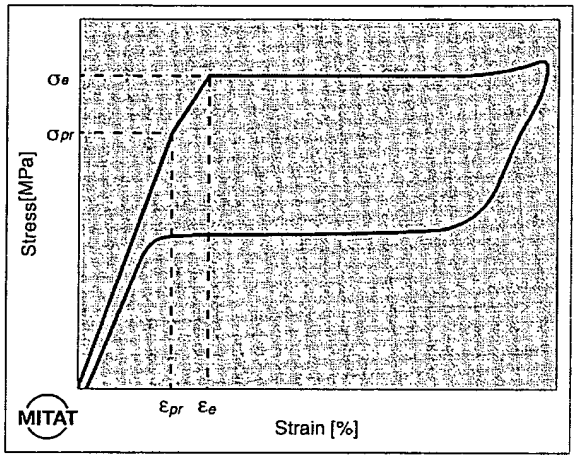

Figure 14. A schematic stress–strain curve of a superelastic Ni-Ti alloy that illustrates the proportional stress limit (σ_{pr}) and the critical stress to induce the martensitic transformation (σ_M) and corresponding strains.

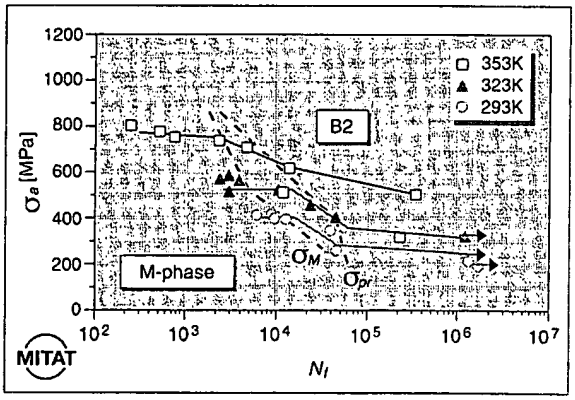

Figure 15. The data from Figure 13 are re-plotted to show the influence of stress on the fatigue life of Ti-50.9at%Ni alloys. Note that the stress endurance limit is a function of test temperature. The proportional stress limit (σ_{pr}) and the critical stress to induce the martensitic transformation (σ_M) are indicated on the figure. (After Kim and Miyazaki, Ref. 26.)

plotted against the difference between test temperature and transformation temperature, T-A_f. As highlighted by Stöckel [2], analysis of the delta between the test temperature and transformation temperature can be a powerful design tool. For example, we can extrapolate the data from constant A_f material tested at different temperatures to understand the behaviour of different transformation temperatures at a constant (body) temperature.

Conclusions

The goals of this paper were to correlate the properties of Ti–Ni alloys with processing, and to address three relevant questions frequently posed by design engineers. Optimised Ti-50.8at%Ni wire was manufactured according to industry standards by precise control of the composition, cold work and continuous strain-age annealing. We can summarise the details presented here by answering the questions posed in the introduction:

Are the mechanical properties constant over a wide range of temperatures?

As shown in Figure 5, the mechanical properties vary over a 300°C temperature range (−100°C to 200°C). Measurement of the permanent set provides a 'superelastic window' where there is minimal residual strain. Within this window, it was also demonstrated that the plateau stresses are directly related to the test temperature and transformation temperature. Therefore, the plateau stress of wire can be readily determined for a given A_f temperature. It was also discussed that the corollary is also true: for a given test temperature, the plateau stresses can be calculated for wires with different transformation temperatures. The important message from this is that the A_f, test temperature, and wire 'stiffness' can not be manipulated independently.

Can we adjust the transformation temperature without modifying the mechanical properties?

As discussed in the previous question, thermal treatments that modify the A_f temperature will also affect the other mechanical properties, especially the plateau stresses. It was shown, however, that the transformation temperature, and hence the properties, can be accurately tuned by selective ageing treatments.

Do the shape-memory and superelastic properties imply that Nitinol has an infinite fatigue life?

The fatigue properties of Ti–Ni wire were shown to depend on the mode of deformation, which, in turn, is a function of the relative stress, strain and test temperature. Higher endurance limits were found for the lowest test temperature conditions. It is recommended that fundamental fatigue tests be run in conjunction with pulsatile testing of medical devices.

References

1 Hunter JG, Sackier JM. In: Hunter JG, Sackier JM, editors. *Minimally invasive surgery.* New York: McGraw-Hill, 1993: 3.

2 Stöckel D. Nitinol medical devices and implants. *Min Invasive Ther Allied Technol* 2000; **9**:

3 Frank TG, Xu W, Cuschieri A. Instruments based on shape memory alloy properties for minimal access surgery: interventional radiology and flexible endoscopy. *Min Invasive Ther Allied Technol* 2000; **9**:

4 Funakubo H, ed. *Shape memory alloys,* New York: Gordon and Breach Science Publishers, 1984.

5 Duerig TW, Melton KN, Stöckel D, Wayman CM, editors. *Engineering aspects of shape memory alloys.* London: Butterworth-Heinemann, 1990.

6 Schüßler A. In: Pelton AR, Hodgson D, Russell SM, Duerig T, editors. *Proceedings 2nd International Conference on Shape Memory and Superelastic Technologies (SMST);* Pacific Grove: MIAS, 1997: 143–8.

7 Buchaillot L, Nakamura Y, Ataka M, Fujita H. In: Pelton AR, Hodgson D, Russell SM, Duerig T, editors. *Proceedings 2nd International Conference on Shape Memory and Superelastic Technologies (SMST);* Pacific Grove: MIAS, 1997: 183–6.

8 Hodgson D, Russell SM. Nitinol melting, manufacture and fabrication. *Min Invasive Ther Allied Technol* 2000; **9**:

9 Harrison JD. In: Duerig TW, Melton KN, Stöckel, Wayman CM, editors. *Engineering aspects of shape memory alloys.* London: Butterworth-Heinemann, 1990: 106–111.

10 Yu W. The application of thermal analysis in the study of ni-ti shape memory alloys. In: Shull RD and Joshi A, editors. *Thermal analysis in metallurgy.* Warrendale, PA: AIME, 1992: 187–204.

11 Marquez J, Slater T, Sczerzenie F. Determining the transformation temperatures of niti alloys using differential scaning calorimetry. In: Pelton AR, Hodgson D, Russell SM, Duerig T, editors. *Proceedings 2nd International Conference on Shape Memory and Superelastic Technologies (SMST);* Asilomar 1997: 13–18.

12 Chen JT, Duerig TW, Pelton AR, Stöckel D. An apparatus to measure the shape memory properties of nitinol tubes for medical applications. *J de Physique IV Coll C8*: 5: 1247–52.

13 Rice C and Sczerzenie F. Design and performance of a functional A_f tester. In: Pelton AR, Hodgson D, Russell SM, Duerig T, editors. *Proceedings 2nd International Conference on Shape Memory and Superelastic Technologies (SMST);* Pacific Grove: MIAS, 1997: 19-22.

14 Otsuka K. Introduction to the r-phase transition. In: Duerig TW, Melton KN, Stöckel D, Wayman CM, editors.

Engineering aspects of shape memory alloys. London: Butterworth-Heinemann, 1990: 36–45.
15 Tamura I, Wayman CM. Martensitic transformations and mechanical effects. In: Olson GB and Owen WS, eds. *Martensite*. ASM International, 1992: 227–42.
16 Shimizu K, Tadaki T. Shape memory effect: mechanism. In: Funakubo H, ed. *Shape memory alloys*, New York: Gordon and Breach Science Publishers, 1984: 1–60.
17 Stöckel D,Yu W. Superelastic ni-ti wire. *Wire J Int* 1991; 45–50.
18 Duerig TW, Zadno R. An engineer's perspective of pseudoelasticity. In: Duerig TW, Melton KN, Stöckel D, Wayman CM, editors. *Engineering aspects of shape memory alloys*. London: Butterworth-Heinemann, 1990: 369–93.
19 Miyazaki S. Thermal and stress cycling effects and fatigue properties of ni-ti alloys. In: Duerig TW, Melton KN, Stöckel D, Wayman CM, editors. *Engineering aspects of shape memory alloys*. London: Butterworth-Heinemann, 1990: 394–413.
20 Nishida M, Wayman CM, Honma T. Precipitation processes in near-equiatomic tini shape memory alloys. *Met Trans* 1986; **17A**: 1505–15.
21 Aaronson H, Lee Y, Russell KC. Diffusional nucleation and growth. In: Russell KC, Aaronson HI, editors. *Precipitation processes in solids*, Warrendale, PA: AIME, 1978: 31–86.
22 Melton KN. Ni-Ti based shape memory alloys. In: Duerig TW, Melton KN, Stöckel D, Wayman CM, editors. *Engineering aspects of shape memory alloys*. London: Butterworth-Heinemann, 1990: 21–35.
23 *Guidance for the submission of research and marketing applications for interventional cardiology devices*. US Department of Health and Human Services, FDA 1995.
24 Pedersen OM, Aslaksen A, Vik-Mo H. Ultrasound measurement of the luminal diameter of the abdominal aorta and iliac arteries in patients without vascular disease. *J Vasc Surg* 1993; **17**: 596–601.
25 Melton KN, Mercier O. Fatigue of niti thermoelastic martensites. *Acta Metall* 1979; **27**: 137–44.
26 Kim YS, Miyazaki S. Fatigue properties of ti-50.9at%ni shape memory wires. In: Pelton AR, Hodgson D, Russell SM, Duerig T, editors. *Proceedings 2nd International Conference on Shape Memory and Superelastic Technologies (SMST);* Pacific Grove: MIAS, 1997: 473–7.
27 Miyazaki S, Mizukoshi K, Mizukoshi, *et al.* Fatigue life of ti-50at%ni and ti-40ni-10cu(at%) shape memory alloy wires. *Mat Sci Eng A* 1999; **273–275**: 658–63.
28 Glenn R, Lee J. Accelerated pulsatile fatigue testing of ni-ti coronary stents. In: Pelton AR, Hodgson D, Russell SM, Duerig T, editors. *Proceedings 2nd International Conference on Shape Memory and Superelastic Technologies (SMST);* Pacific Grove: MIAS, 1997: 585–90.
29 Dauskardt RH, Duerig TW, Ritchie RO. Effects of *in-situ* phase transformations on fatigue-crack propagation in titanium-nickel shape memory alloys. *MRS Intl Mtg Adv Mat* 1989: **9:** 243–9.